

## Photoexcited solitons and polarons in pernigraniline-base polymers

J. M. Leng,\* R. P. McCall,<sup>†</sup> and K. R. Cromack<sup>‡</sup>

*Department of Physics, The Ohio State University, Columbus, Ohio 43210-1106*

Y. Sun,<sup>§</sup> S. K. Manohar,<sup>||</sup> and A. G. MacDiarmid

*Department of Chemistry, University of Pennsylvania, Philadelphia, Pennsylvania 19104-6323*

A. J. Epstein

*Department of Physics and Department of Chemistry, The Ohio State University, Columbus, Ohio 43210-1106*

(Received 11 June 1993)

We present results of absorption, near-steady-state and long-time photoinduced absorption, and light-induced electron-spin resonance (LESR) studies for the pernigraniline-base polymer (PNB), which has a Peierls ground state with multiple order parameters. Two kinds of defects have been observed and differentiated by photoinduced-absorption spectroscopies in different time domains, namely polarons and solitons. Direct absorption of PNB shows the Peierls energy gap at 2.3 eV and  $\pi-\pi^*$  transition energies at 3.8 and 4.3 eV. Pumping at 2.41 eV (into the Peierls gap), the near-steady-state photoinduced absorption spectrum at room temperature shows three induced absorption peaks at 1.0 eV (LE), 1.5 eV (ME), and 3.0 eV (HE); at a temperature of 10 K, the LE peak becomes two peaks at 1.0 eV (LE1) and 1.3 eV (LE2). With pump photon energy of 3.8 eV (into the  $\pi-\pi^*$  gap) and at 10 K, features similar to those observed by pumping into the Peierls gap were found, except the intensity of each of the features increased by a factor of 4. The LE features are short lived with a lifetime on the millisecond time scale and have associated short-lived infrared vibrations. The ME peak is very long lived; in addition, there are very long-lived, relatively weak infrared vibrations. The lifetime of the ME peak is measured to be greater than 24 h for temperatures below 200 K. The defect masses for long-lived and short-lived defects are estimated to be  $\sim 300m_e$  and  $\sim (5-10)m_e$ , respectively, using the amplitude-mode formalism. Light-induced ESR studies show the long-lived 1.5 eV peak has spin while the short-lived defect has no spin. We suggest that the LE peaks originate from charged soliton-antisoliton pairs (dominated primarily by the bond-length order parameter  $u$ ), while the ME peak originates from massive ring-torsional polarons (with dominant ring-torsion-angle order parameters  $\delta$  and  $\Psi_0$ ).

### I. INTRODUCTION

Pernigraniline-base polymer (poly-*paraphenylene imine*), the fully oxidized state of polyaniline, is proposed to be a ring-containing Peierls system.<sup>1-4</sup> Polyaniline was first synthesized and studied chemically nearly a century ago,<sup>5</sup> although it has been the focus of increased physical and chemical studies only in the past several years.<sup>6</sup> It has been demonstrated<sup>7</sup> that pristine polyaniline may be prepared in three discrete oxidation states, namely, leucoemeraldine base (LEB), emeraldine base (EB), and pernigraniline base (PNB), depicted in Fig. 1, each of the oxidation states of polyaniline having novel physical and chemical properties. The intermediate oxidation state, emeraldine base, and its doped (protonated) form have been studied most extensively.<sup>6</sup> For example, emeraldine base can be converted from an insulator to a conductor upon protonic acid doping with hydrochloric acid.<sup>8-16</sup> The origin of the high-conductivity state of emeraldine salt (ES) was proposed to be an insulator-to-metal transition concomitant with the formation of a polaron lattice upon protonation of EB.<sup>9</sup> Photoinduced absorption of EB revealed that hole polarons and molecular excitons are the main defect states observed upon photoexcitation.<sup>17</sup>

Leucoemeraldine and pernigraniline bases have been less studied than emeraldine base, partly due to the fact that leucoemeraldine and pernigraniline bases are less readily synthesized and, once made, are less stable in air than emeraldine base. Recently, these two forms of polyaniline have been successfully synthesized and charac-

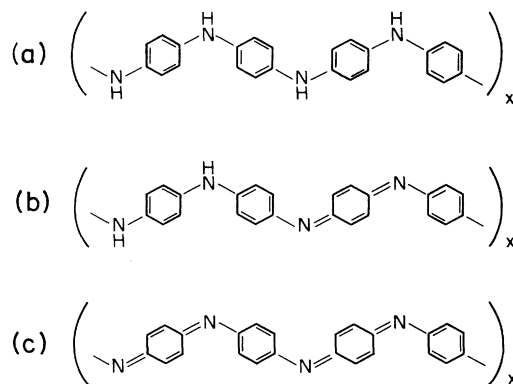


FIG. 1. Chemical structure of (a) leucoemeraldine base (LEB), (b) emeraldine base (EB), and (c) pernigraniline base (PNB).

terized.<sup>18,19</sup> A new type of hole polaron, namely, a ring-torsional polaron<sup>2,3</sup> similar to a Holstein polaron,<sup>20</sup> was proposed to be responsible for photoinduced defect states in LEB.<sup>3</sup> Photoinduced absorption<sup>21</sup> of both LEB and EB exhibits long-lived defect states with an absorption peak at  $\sim 1.4$  eV, which have been described in terms of polarons bound to quinoid rings,  $P_{BQ}^+$ .<sup>21</sup>

The richness of the polyaniline family has been more evident since chemically pure pernigraniline-base polymer has become available.<sup>18,22</sup> The chemical structure of PNB suggests that pernigraniline base is a Peierls systems that possesses a doubly degenerate ground state. Unlike LEB, of which the simplest repeat unit consists of a benzenoid ring and NH group (for a total of eight  $p_z$  electrons and resulting filled energy bands), the simplest repeat unit of PNB consists of one  $C_6$  ring and one nitrogen atom (for a total of seven  $p_z$  electrons and a half-filled highest-occupied energy band). Such a structure is unstable with respect to forming a dimerized structure. Figure 2 illustrates the proposed chemical structure of pernigraniline base without and with dimerization. In the dimerized case, pernigraniline base has alternating benzenoid and quinoid rings between nitrogen atoms. By interchanging the benzenoid and quinoid rings, a topologically identical structure can be constructed. Therefore pernigraniline base is the first polymeric Peierls system with a degenerate ground state beyond *trans*-polyacetylene. Quantum chemical calculations<sup>1</sup> and Hückel model calculations<sup>2-4</sup> favor such a dimerized structure. In analogy to *trans*-polyacetylene, pernigraniline base has a dimerization. In the simplest approach, the resulting alternating single and double carbon-carbon and nitrogen-carbon bonds can be described by the bond-length order parameter  $u$ , i.e., the deviation from uniform bond lengths.

Recently, the central role of the ring-torsion-angle degree of freedom in ring-containing polymers was proposed.<sup>2,3</sup> In addition to its dependence on the bond-length order parameter, the transfer integral between nitrogen  $p_z$  orbitals and the ring  $\pi$  orbitals has a cosine dependence on the torsion angles  $\Psi_0$  ( $\Psi_0=0$  implies that

the  $C_6$  ring is in a plane defined by the N atoms resulting in a maximum transfer integral;  $\Psi_0=90^\circ$  implies that the  $C_6$  ring is twisted perpendicular to the plane of the N's and that the transfer integral is zero). Instead of alternating ring-torsion angles alternating as  $\pm\Psi_0$  and  $\mp\Psi_0$  to reduce steric repulsion as in LEB, the PNB ring-torsion angle is suggested to alternate, varying as  $\pm\Psi_0\pm\delta$  and  $\mp\Psi_0\pm\delta$ , where  $\Psi_0$  is the average ring-torsion angle of benzenoid and quinoid rings in PNB and  $\delta$  is the deviation from the average ring angle. Ginder and Epstein proposed that this ring-angle alternation is one source that is responsible for the Peierls ground states and defect states, namely, ring-torsional dimerization and ring-torsion-dominated solitons and polarons.<sup>2,3</sup> The defect mass has been estimated to be very large ( $> 100m_e$ ) when the deformation in  $\delta$  contributes substantially to the defect states. Recently, Brédas *et al.*<sup>23</sup> calculated that the Peierls gap of PNB is linearly proportional to both  $u$  and  $\delta$ , with the presence of both order parameters contributing nearly equal amounts to the band gap. It is noted that the phases and magnitudes of  $u$  and  $\delta$  are expected to be coupled because the quinoid rings ( $-u$ ) are expected to have a lower-energy configuration if they lie closer to the plane of the nitrogens ( $-\Psi_0+\delta$ ).

We present here the photoexcitation spectra [or photoinduced absorption (PA)] and light-induced electron spin resonance (LESr) of the pernigraniline-base polymer extending our earlier preliminary reports<sup>24-26</sup> on this system. Our results show that two kinds of photoinduced defects are found in the PNB, namely, long- and short-lived defects. The short-lived defects (millisecond time scale, studied from  $800\text{ cm}^{-1}$  to  $3.4\text{ eV}$ ) are proposed to be of solitonic origin involving primarily the order parameter  $u$  (bond-length changes), while the long-lived defect (lifetime greater than seconds, studied from  $500$  to  $13\,000\text{ cm}^{-1}$ ) is proposed to be polaronic in origin with substantial contribution from the order parameter  $\delta$  (ring-torsion-angle changes). An amplitude-mode analysis<sup>27</sup> of the photoinduced infrared-active vibrational (IRAV) modes and the photoinduced electronic transitions shows that the effective mass of the long-lived polaron is very large ( $\sim 300m_e$ ), while that of the short-lived soliton is modest ( $\sim 5m_e$ ). These results indicate the importance of ring-torsion angle and bond-order dimerization in pernigraniline base.

The remainder of the paper is organized as follows. Experimental techniques will be discussed in the next section with experimental results for direct absorption, photoinduced absorption, and light-induced electron-spin resonance presented in Sec. III. The data will be discussed in Sec. IV and conclusions given in Sec. V.

## II. EXPERIMENTAL TECHNIQUES

### A. Sample preparation

In a typical preparation of pernigraniline base,<sup>18</sup>  $\sim 1$  g of emeraldine base was dissolved in a solution of N-methyl-pyrrolidone (NMP, 100 ml) mixed with glacial acetic acid (5 ml). A glacial acetic acid solution (10 ml) containing purified *m*-chloroperbenzoic acid (0.72 g) was

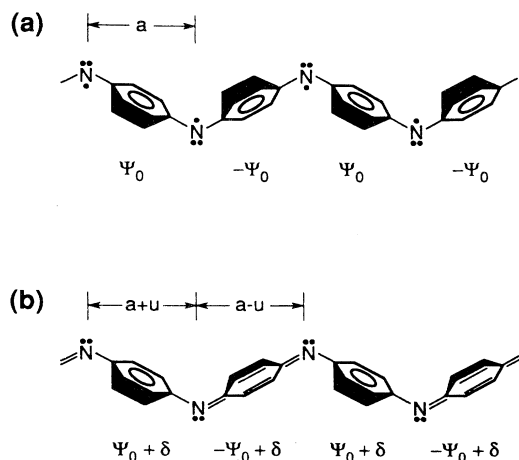


FIG. 2. Schematic illustrations of the proposed structure of PNB: (a) undimerized and (b) dimerized.

added in 1 ml portions every 10 min. A dark violet solution was observed after stirring at room temperature for an additional 15 min. Triethylamine (10 ml) was added to produce a dark purple partially crystalline precipitate of PNB with a coherence length of up to 40–50 Å.<sup>28</sup>

Samples in both powder and thin-film forms were used in optical and light-induced electron-spin-resonance (ESR) experiments. Powder samples were mixed with KBr in less than 0.1% by weight ratio. This mixture was then ground and pressed into an optical quality pellet at a pressure of  $3.3 \times 10^8$  Pa. In near-steady-state photoinduced absorption (PA), light scattered from the pressed pellet samples can complicate the PA experiment for probe photon energy above 2.0 eV. Therefore, in this spectral range ( $h\nu > 2.0$  eV), samples cast as films on either glass or quartz substrates were used. For probe photon energy in the mid-IR range (500–20 000  $\text{cm}^{-1}$ ), the pressed pellet samples were used for both long-time [Fourier-transform-infrared (FTIR)] or near-steady-state photoinduced-absorption experiments. The samples were handled in an inert environment (argon gas) or under vacuum during all stages of the experiments as the PNB samples degrade in air.

### B. Direct absorption

Direct-absorption spectra were measured with a Perkin-Elmer Lambda 9 UV/Vis/NIR spectrophotometer in the range of 900–190 nm (1.4–6.0 eV), as well as with a home-built UV/Vis/NIR spectrophotometer in the range of 1500–190 nm (0.7–6.0 eV). In the home-built UV/Vis/NIR spectrophotometer, a 100-W tungsten-halogen lamp was used in the near-IR to UV range (0.3–3.3 eV) and a deuterium lamp was used in the UV range (2.5–6.0 eV). The transmitted light was dispersed by a  $\frac{1}{4}$ -m monochromator. UV-enhanced silicon (1.1–6 eV) and indium arsenide (InAs) (0.5–2.0 eV) photodiodes were used to record the incident light at the exit slit of the monochromator. The samples were dissolved in NMP solution or cast into thin films on substrates to take the absorbance spectra. Direct-absorption measurements were routinely employed for several reasons: First, it provides a measure of the ground oxidation state of the sample; only those samples without degradation were selected for further studies in the PA experiment; and second, to check the heating-induced absorption changes of the sample. All the spectra reported in this paper were checked for effects of heating (determined by comparing transmission at, for example, 200 and 300 K). Unless otherwise specified, the features reported in this paper are intrinsic in origin.

### C. Photoinduced absorption

Photoinduced-absorption (PA) results were obtained via two different approaches. (1) The near-steady-state PA experiment employed the same  $\frac{1}{4}$ -m grating monochromator that was used for direct absorption to disperse the probe light. A Spectra-Physics model 171 argon-ion laser, a Spectra-Physics model 301 dye laser (1.94–2.21 eV), or a Photon Technology International Inc. Hg-Xe

arc lamp (3.8 eV) was chopped by a mechanical chopper at 4–4000 Hz. The probe light, which can be a 100-W tungsten-halogen lamp (0.3–3.3 eV), a globalar (0.1–0.3 eV), or a deuterium lamp (2.5–6.0 eV), was focused onto the sample that was mounted in a CTI-Cryogenics closed-cycle cryostat (10–350 K). The probe light was detected by a UV-enhanced Si (1.1–6.0 eV), an InAs (0.5–2.0 eV), or a MCT/InSb two-color detector (0.1–1.2 eV). (2) The long-time photoinduced-absorption experiments were carried out on a Nicolet 60SX Fourier-transform-infrared (FTIR) spectrometer (500–20 000  $\text{cm}^{-1}$ ). The pump beam (a Coherent Innova 70 argon-ion laser or Coherent CR-599 dye laser) was guided into the sample chamber and was blocked and unblocked by a mechanical shutter. The transmission spectrum ( $S_0$ ) was measured before the sample was exposed to the pump beam. After exposure to the pump beam for a typical time of 20 sec, a second transmission spectrum ( $S_1$ ) was measured again. The relative changes in transmission ( $S_0 - S_1$ )/ $S_0$  were then computed. For the long-time experiments, samples were maintained in a cryostat for control of temperature in the range of  $\sim 10$ –320 K.

### D. LESR

The LESR experiment utilized a Bruker 300 ESP electron-paramagnetic-resonance (EPR) X-band spectrometer with an optical access cavity. Temperature control was provided by an Oxford 900 system. A cw Coherent Innova 70 argon-ion laser or a Coherent CR-599 dye laser pump beam was routed to the ESR cavity through a 200- $\mu\text{m}$  single fiber-optic cable. A Hg-Xe arc lamp was used to pump the sample in the UV region (3.8 eV). Typically, two methods were used in the LESR experiments: (1) double modulation by mechanically chopping the pump beam and modulating the magnetic field at  $10^5$  Hz to obtain the photoinduced change in the EPR derivative signal and (2) single modulation with a direct comparison of the EPR derivative spectrum obtained with the pump beam blocked and unblocked. The double-modulation technique gives information concerning spins corresponding to the defects detected in the near-steady-state PA experiment, while the single-modulation technique detects the spins associated with the defects detected in the long-time PA experiment. A reference value for the absolute number of photoinduced spins was obtained by using a home-built Faraday balance<sup>9,26</sup> to determine the number of spins present in PNB in the absence of photoexcitation.

## III. EXPERIMENTAL RESULTS

### A. Direct absorption

The direct-absorption spectrum in the range 1.4–5 eV of PNB in NMP solution is compared with that of EB in NMP solution in Fig. 3. The PNB absorption spectrum shows a peak at  $\sim 2.3$  eV with an onset of absorption at  $\sim 1.8$  eV. This peak is shifted up in energy by 15% and is almost twice as broad as the corresponding peak in EB. Two other maxima were observed at 3.8 and 4.3 eV.

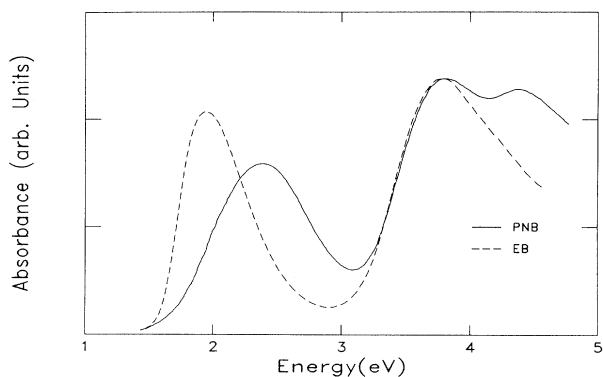


FIG. 3. Absorbance spectra in the near-IR to ultraviolet region of solutions of EB (dashed line) and PNB (solid line) in NMP.

The infrared-absorption spectra of powder samples of LEB, EB, and PNB pressed in pellets of KBr are shown in Fig. 4. Of these oxidation states, PNB has the richest spectrum with strong maxima observed at 848, 1106, 1164, 1215, 1318, 1485, and 1585  $\text{cm}^{-1}$ .

## B. Photoinduced absorption

### 1. Near-steady-state PA

The near-steady-state photoinduced-absorption spectra of PNB in the range 0.5–3.3 eV at temperatures of 300 and 10 K (Fig. 5) were obtained with a pump-laser energy of 2.41 eV, near the Peierls gap of PNB. The laser beam was mechanically chopped at 22.5 Hz. The spectrum at 300 K shows three photoinduced-absorption (PA) features, namely, a low-energy peak (LE) at 1.0 eV, a middle-energy peak (ME) at 1.5 eV, and a high-energy peak (HE) at 3.0 eV; and a photoinduced-bleaching (PB) feature maximum at 2.0 eV. At a temperature of 10 K, the original LE peak is replaced by two peaks at 1.0 eV (LE1) and 1.3 eV (LE2). We note that LE1 and LE2 are much stronger than LE, while HE is reduced in strength and shifted to 3.1 eV upon cooling. The onset of the PB feature shifts downward in energy by 0.1 eV, and its relative oscillator strength decreases at the lower temperature.

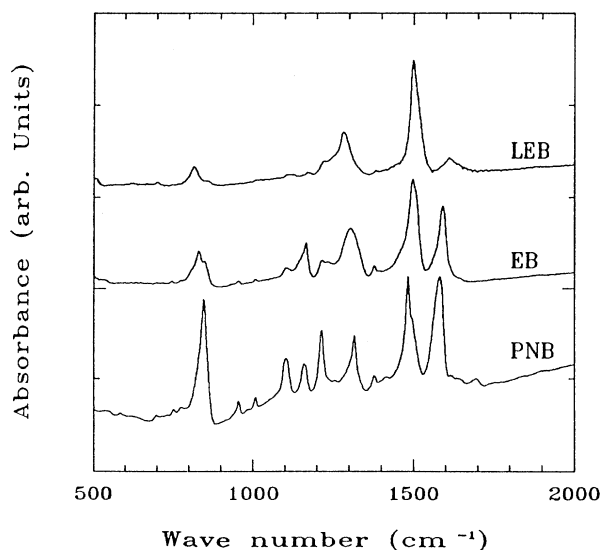


FIG. 4. Infrared absorbance of LEB, EB, and PNB powder samples in pressed KBr pellets.

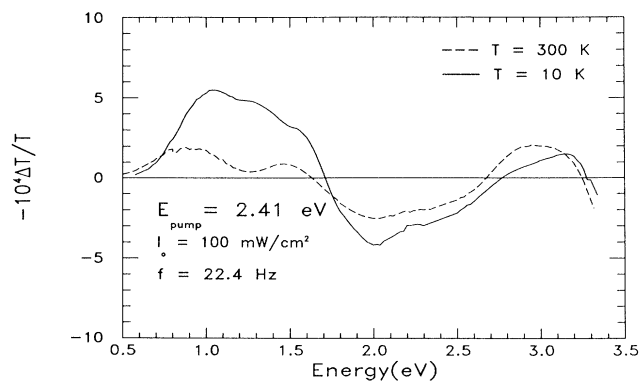


FIG. 5. Near-steady-state photoinduced-absorption spectra of a PNB thin-film sample at 300 K (dashed line) and 10 K (solid line). The sample was pumped at 2.41 eV with a pump intensity of 100  $\text{mW}/\text{cm}^2$ .

The near-steady-state PA spectra with pump energy of 3.8 eV at 10 K (Fig. 6) demonstrates similar features as those observed by pumping near the Peierls gap. There is a broad LE feature centered at 1.1 eV, a ME feature at  $\sim 1.6$  eV, and a HE feature at  $\sim 3.1$  eV. A photoinduced-bleaching peak is observed at 2.0 eV. Although the power of the incident pump photon beam increased by 40% (decrease in photon flux of 10%), the intensity of each photoinduced peak is increased by a factor of 4.

The near-steady-state PA experiment was extended to the IR range (0.1–2.0 eV). Figure 7 shows the 10-K near-steady-state PA of PNB in powder form mixed with KBr ( $\sim 0.05\%$ ) in the midinfrared range (1000–12 500

The near-steady-state PA experiment was extended to the IR range (0.1–2.0 eV). Figure 7 shows the 10-K near-steady-state PA of PNB in powder form mixed with KBr ( $\sim 0.05\%$ ) in the midinfrared range (1000–12 500

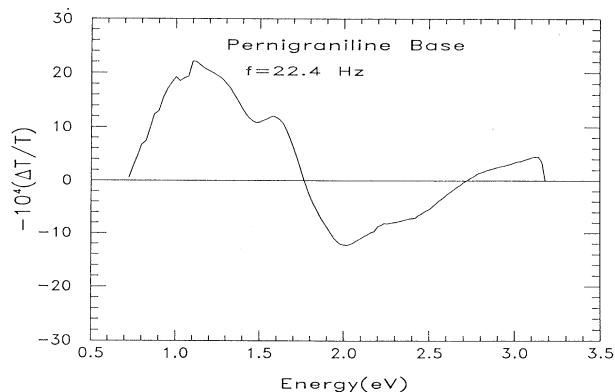


FIG. 6. Near-steady-state photoinduced-absorption spectrum of a PNB thin-film sample pumping into the  $\pi-\pi^*$  gap (3.8 eV excitation) at a temperature of 10 K with a pump intensity of 140  $\text{mW}/\text{cm}^2$ .

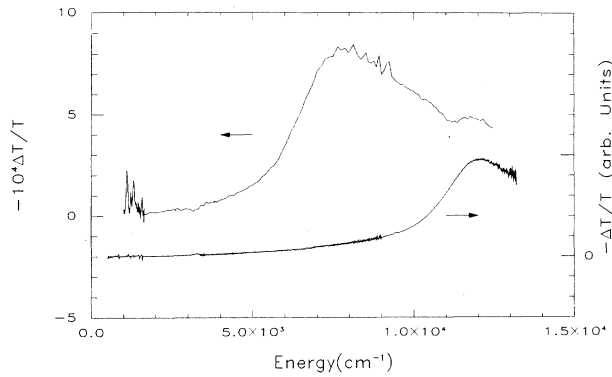


FIG. 7. Near-steady-state (upper curve) and long-time (lower curve) PA of PNB powder samples. The long-time PA signal was reduced  $\sim 400$  times to match the size of the 1.5-eV ME feature in the near-steady-state PA experiment. The near-steady-state PA experiment was carried out with pump intensity of 250 mW/cm<sup>2</sup>, chopper frequency of 22.4 Hz, and sample temperature of 10 K. The long-time PA experiment was carried out with pump intensity of 100 mW/cm<sup>2</sup> and sample temperature of 80 K.

cm<sup>-1</sup> or 0.1–1.6 eV) with a pump-beam photon energy of 2.41 eV and an intensity of 250 mW/cm<sup>2</sup>. PA peaks were found at 8000 cm<sup>-1</sup> (1.0 eV) and 12000 cm<sup>-1</sup> (1.5 eV). A shoulder is also seen at  $\sim 10000$  cm<sup>-1</sup> ( $\sim 1.3$  eV). This spectrum is in good agreement with that of Fig. 5, which represents a similar experiment performed on thin-film samples. Photoinduced IRAV modes were found at 1100, 1220, 1320, and 1580 cm<sup>-1</sup>. No photoinduced-bleaching modes were observed in the near-steady-state PA spectra.

## 2. Long-time PA

The long-time PA data for a sample of PNB powder in KBr at 80 K, optically pumped by a laser beam of 2.54 eV and 100 mW/cm<sup>2</sup>, are shown in Fig. 7 together with the short-time PA spectrum. In the long-time spectrum, only one peak is observable at 12000 cm<sup>-1</sup> (1.5 eV), while the 1.0- and 1.3-eV features are completely absent. The long-time photoinduced infrared-active vibrational (IRAV) modes are small compared to the ME feature. The IRAV parts of the spectra of both near-steady-state and long-time PA are plotted together in Fig. 8. For the long-time PA spectrum, three major PA features were observed in the mid-IR range at 1153, 1477, and 1554 cm<sup>-1</sup>. Photoinduced-bleaching (PB) features were observed at 1219, 1323, 1487, and 1591 cm<sup>-1</sup>. Figure 9 shows the decay of the long-time feature at 1.5 eV for the sample held at 10 K for up to 3 h. Note that there is very little decay after 1 h. Measurements at times up to 24 h show no further decay of the PA signal at temperatures as high as 200 K.

## C. Time dynamics of the photoinduced absorption

In the near-steady-state PA experiment, the dependence of the photoinduced signal on pump-laser power

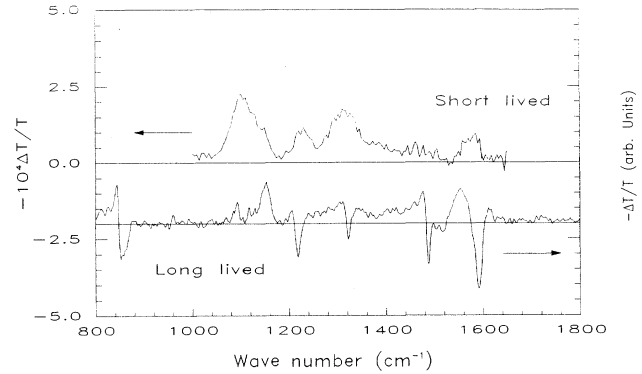


FIG. 8. Photoinduced IRAV modes of PNB observed by near-steady-state PA (upper curve) with pump photon energy of 2.41 eV, intensity of 250 mW/cm<sup>2</sup>, chopper frequency 22.4 Hz, and sample temperature of 10 K. Photoinduced IRAV modes of PNB observed in the long-time PA experiment (lower curve) with pump photon energy of 2.54 eV, intensity of 100 mW/cm<sup>2</sup>, and sample temperature of 80 K. The long-time PA spectrum has been reduced by a factor of 250.

and chopper frequency provides insight into the time dynamics of the photoexcited defects. In the near-steady-state PA experiment, the number of defects is determined by two factors, the photogeneration and recombination rates. A simplified rate equation for the number of defects  $n$  can be written

$$\frac{dn}{dt} + \frac{n^v}{\tau} = \alpha I, \quad (1)$$

where  $\tau$  is the lifetime of the defects,  $v$  is determined by

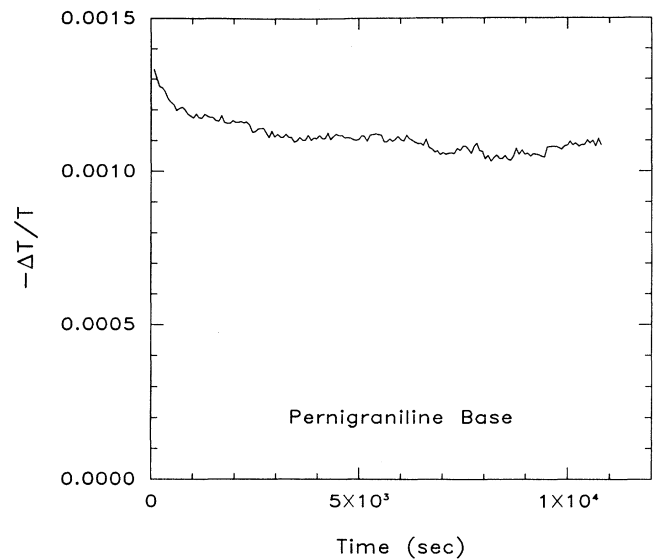


FIG. 9. Time evolution of the 1.5-eV (ME) near-steady-state PA peak of the PNB powder sample mixed with KBr at 10 K. The PA signal was monitored with time for up to 3 h after first cooling the sample in the dark, then turning the chopped laser on. The laser photon energy was 2.41 eV, intensity 200 mW/cm<sup>2</sup>, and frequency 22.5 Hz.

the type of decay processes with  $\nu=1$  for unimolecular decay and  $\nu=2$  for bimolecular decay,  $I$  is the time-dependent pump photon flux, which can be approximated by a square wave that switches between some constant flux  $I=I_0$  and  $I=0$  at frequency  $f$ , and  $\alpha$  is a constant.

Assuming a unimolecular recombination process, the rate equation can be solved for the square-wave case. During the half of the cycle when the pump beam is incident on the sample,

$$n = \alpha I_0 \tau (1 - e^{-t/\tau}) + n_0 e^{-t/\tau}, \quad (2)$$

where  $n_0$  is the number of defects at time  $t=0$ . Similarly, for the half of the cycle when the pump beam is not on the sample,

$$n = n'_0 e^{-t'/\tau}, \quad (3)$$

where  $n'_0$  is the number of defects present when the pump beam is turned off at a time  $t'=0$ . The number of defects can be calculated for all times, and after many periods (for long exposure times) the difference in the number of excitations that exist at the end of each half period of the pump beam on and the pump beam off,  $\Delta n$ , can be determined. This case is the near-steady-state condition, and we find

$$\Delta n = \alpha I_0 \tau \frac{(1 - e^{-1/2\tau f})^2}{1 - e^{-1/\tau f}}, \quad (4)$$

where  $f$  is the frequency of the chopped pump beam. The value of  $\Delta n$  is proportional to the signal observed at the lock-in amplifier. The derived expression shows that for unimolecular decay the signal depends linearly on the photon flux. At high chopping frequencies or long lifetimes (i.e., the lifetime is much longer than the period), the signal varies as  $\Delta n = \alpha I_0 / 4f$ , i.e., proportional to  $f^{-1}$ . Conversely, for low chopping frequency or very short lifetime (i.e., the lifetime is much shorter than the period), the signal varies as  $\Delta n = \alpha I_0 \tau$ , which is independent of frequency.

Similar results hold for bimolecular recombination in the square-wave excitation case. During the half cycle when the pump beam is incident on the sample, the rate equation can be solved to give

$$n = \frac{n_0 + \sqrt{\alpha I_0 \tau} \tanh[(\sqrt{\alpha I_0 / \tau})t]}{1 + (n_0 / \sqrt{\alpha I_0 \tau}) \tanh[(\sqrt{\alpha I_0 / \tau})t]}, \quad (5)$$

where  $n_0$  is the number of defects at time  $t=0$ . Similarly, for the half of the cycle where the pump beam is not on the sample, the solution of the rate equation is

$$n = \frac{n'_0}{1 + n'_0 t / \tau}, \quad (6)$$

where  $n'_0$  is the number of defects present when the pump beam is turned off at time  $t'=0$ . The number of defects can be calculated numerically for all times, and after many periods (for long exposure times) the near-steady-state value for the difference in excitations that exist at the end of each half period of the pump beam on and the pump beam off,  $\Delta n$ , can be determined. The numerically

calculated  $\Delta n$  can be shown to be proportional to the square root of the photon flux,  $\Delta n \propto \sqrt{I_0}$ . Similar to the unimolecular decay case, it is seen that for high chopping frequencies or long lifetimes (i.e., for lifetimes much greater than the period), the signal is inversely proportional to the frequency,  $\Delta n \propto f^{-1}$ . In addition, for low chopping frequency or very short lifetimes (i.e., for lifetimes much shorter than the period), the signal is independent of frequency,  $\Delta n \propto f^0$ .

Similar behavior of the measured photoinduced signal would be expected for other time dependences of the pump beam. For example, if the pump beam incident on the sample were sinusoidal in nature, i.e.,

$$\frac{dn}{dt} + \frac{n^\nu}{\tau} = \alpha I_0 (1 + \sin \omega t), \quad (7)$$

where  $\omega$  is the chopper frequency in rad/sec, the same dependence is found for the signal on chopper frequency: For high chopping frequency the signal varies as  $f^{-1}$ , and for low chopping frequency the signal is independent of frequency.

In the experiments reported here, the chopper frequency was tuned in the range of 4–400 Hz and the magnitude of the PA signal was recorded. An average lifetime  $\tau$  of defects can be estimated from the intersection of the lines of slope  $-1$  at the high-frequency end and of slope 0 at the low-frequency end.

Figure 10 shows the chopper frequency response for a 2.41-eV pump beam. The 1.0-eV (LE1) and 1.3 eV (LE2) PA peaks have essentially the same chopper frequency dependence at 10 K. The effective lifetimes of the LE1 and LE2 peaks are estimated to be  $\sim 0.01$ – $0.1$  sec. The ME and HE peaks have frequency dependence for a frequency range of 4–100 Hz, somewhat different from that of the LE1 and LE2 peaks. To the lowest chopper frequency available (4 Hz) in the near-steady-state

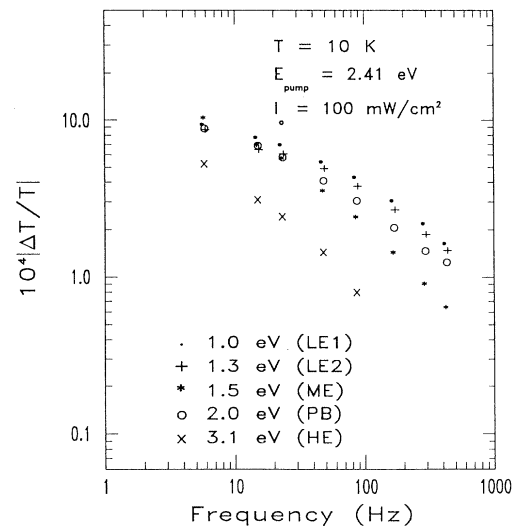


FIG. 10. Chopper frequency dependence of the near-steady-state PA features in PNB film at 10 K: the LE1 peak (●), the LE2 peak (+), the ME peak (\*), the photoinduced-bleaching (PB) peak (○), and the HE peak (×).

photoinduced-absorption experiment, the ME and HE peaks still increase steadily without showing a critical frequency, reflecting that the lifetimes of the ME and HE peaks are much longer than those of the LE features. In the long-time experiment, the lifetimes of the ME (Ref. 29) and the HE (Ref. 30) have been measured to be greater than 24 h at temperatures up to 200 K.

Figure 11 compares the 1.0-eV (LE1), 1.5-eV (ME), and  $1320\text{-cm}^{-1}$  (IRAV) PA intensities versus the chopper frequency (2.41-eV pump) for the PNB sample at 10 K. The IRAV mode has a frequency dependence similar to that of the LE1 peak, indicating that it is associated with the short-lived defect.

The frequency dependence of each photoinduced feature of PNB, obtained by pumping into the  $\pi-\pi^*$  gap (UV excitation), was also studied (Fig. 12). The 1.1-eV peak (LE) shows a saturation at  $\sim 20$  Hz, indicating that the lifetime of the LE feature is  $\sim 0.1$  sec, while the lifetimes of the other features are longer, in agreement with the 2.41-eV pump results.

The dependence of the near-steady-state PA on the pump-laser intensity was also studied (Fig. 13). The magnitudes of all PA features follow a power law of  $I^{-0.7}$ , indicating that the defect decay channels are neither purely unimolecular nor bimolecular in nature. For the UV-pumped PA features (Fig. 14), the power dependence of each feature also shows a dependence with the pump-beam intensity as  $I^{-0.7}$ . This behavior is in marked contrast to the linear dependence on laser intensity for near-steady-state studies of the photoinduced bleaching of the 2-eV (exciton) peak in emeraldine base.<sup>17</sup>

The power dependence of the long-time PA features at  $1153\text{ cm}^{-1}$  and at 1.5 eV (Fig. 15) varies with pump beam intensity as  $I^{-0.6}$ , similar to the near-steady-state experiment. In addition, it is observed that both the 1.5-eV (ME) feature and IRAV modes grow with time under continuous exposure to the pump beam as a stretched exponential.<sup>31</sup>

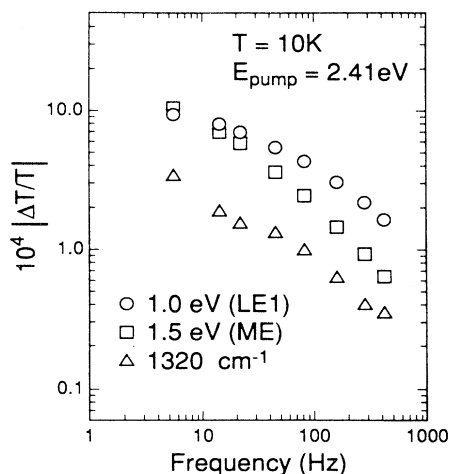


FIG. 11. Chopper-frequency dependence of the near-steady-state PA features in a PNB powder sample: the LE1 peak ( $\circ$ ), the ME peak ( $\square$ ), and the IRAV mode at  $1320\text{ cm}^{-1}$  ( $\triangle$ ).

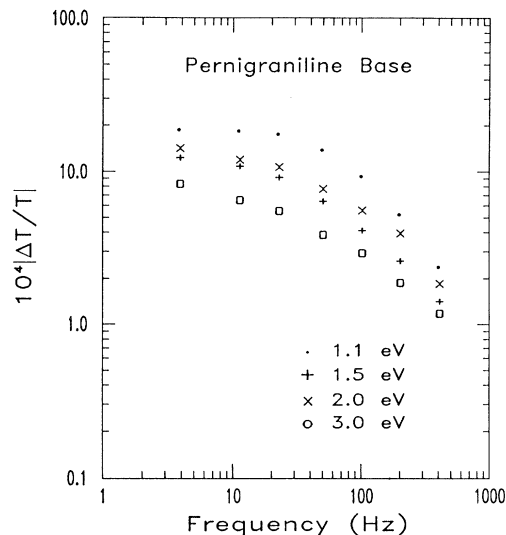


FIG. 12. Chopper frequency dependence of near-steady-state PA features in PNB film pumped at 3.8 eV, temperature of 10 K, and  $I_0 = 140\text{ mW/cm}^2$ : the LE1 peak at 1.1 eV ( $\bullet$ ), the ME peak at 1.5 eV ( $+$ ), the bleaching peak at 2.0 eV ( $\times$ ), and the HE peak at 3.0 eV ( $\circ$ ).

#### D. LESR

The 60-K LESR signal with pump photon energy of 2.54 eV and laser intensity of  $100\text{ mW/cm}^2$  taken with the single-modulation technique is given in Fig. 16. It is easily distinguished from the less intense dark signal.<sup>32</sup> The LESR signal grows with illumination time as a stretched exponential of the form

$$n(t) = A \left\{ 1 - \exp \left[ - \left( \frac{t}{B} \right)^C \right] \right\}, \quad (8)$$

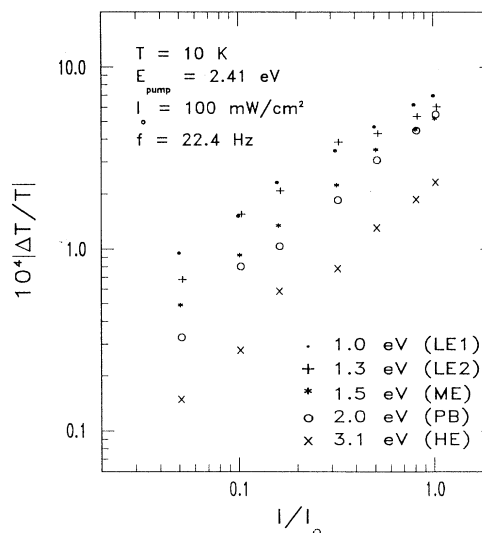


FIG. 13. Pump-beam intensity dependence of the near-steady-state PA features in PNB film for pump-beam energy of 2.41 eV: the LE1 peak ( $\bullet$ ), the LE2 peak ( $+$ ), the ME peak ( $*$ ), the bleaching peak ( $\circ$ ), and the HE peak ( $\times$ ).

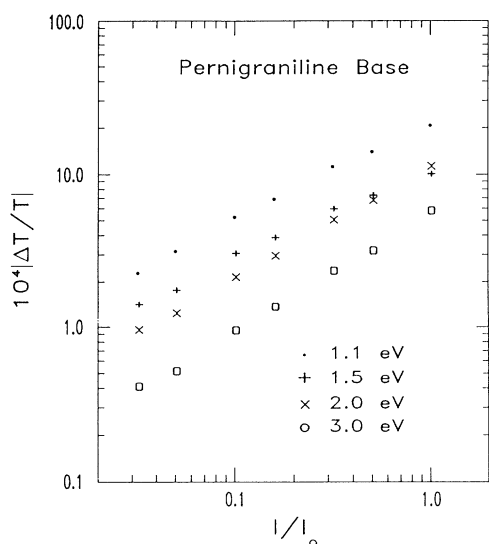


FIG. 14. Pump-beam intensity dependence of the near-steady-state PA features of PNB for pump-beam energy of 3.8 eV,  $I_0 = 140 \text{ mW/cm}^2$ , and sample temperature of 10 K: the LE1 peak ( $\bullet$ ), the ME peak (+), the bleaching peak ( $\times$ ), and the HE peak ( $\circ$ ).

shown in Fig. 17, where for the conditions given the constants  $A$ ,  $B$ , and  $C$  are 11.5, 26.9 min, and 0.56, respectively. The growth of this long-lived signal is similar to the stretched exponential of the 1.5-eV peak and the IRAV modes in the long-time PA experiment.<sup>31</sup>

The dark EPR signal for the PNB sample corresponds to a spin density not exceeding  $2 \times 10^{-3}$  spins/2 rings as determined by the Faraday technique.<sup>32</sup> The double-

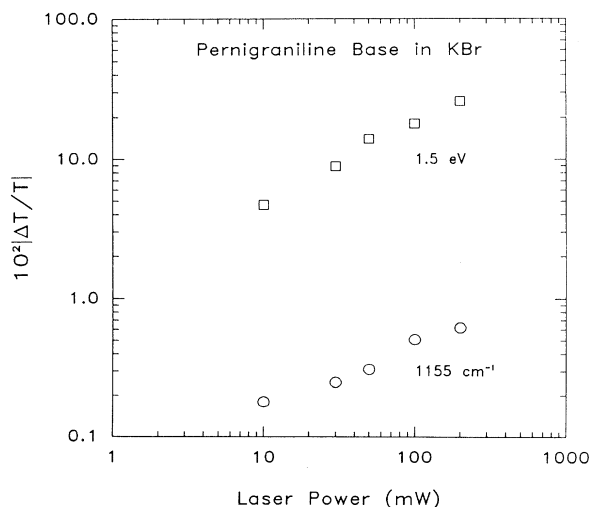


FIG. 15. Pump-beam intensity dependence of the long-time PA features of PNB powder sample in KBr for pump-beam energy of 2.41 eV and sample temperature of 80 K: the  $1155\text{-cm}^{-1}$  IRAV mode ( $\circ$ ) and the ME peak ( $\square$ ). Measurements were made about 20 sec after the pump beam was turned off. The samples were warmed to room temperature between taking data points.

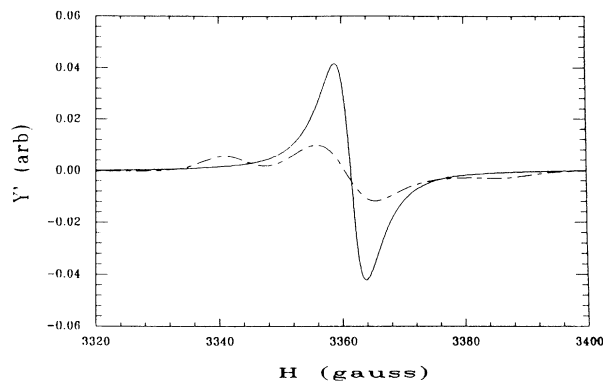


FIG. 16. Long-time LESR signal: dark signal (dashed line) and the light-induced signal (solid line). The data were taken at a sample temperature of 60 K, a laser intensity of  $100 \text{ mW/cm}^2$ , photon energy of 2.54 eV, and after 1 h of laser illumination. The dark signal has been multiplied by a factor of 50 for comparison.

modulated LESR signal (the light source is chopped at a frequency of 5–1000 Hz) was observed to be no larger than 0.05% of the dark EPR signal.<sup>32</sup> Therefore the steady-state photoexcited defect has a spin density no larger than  $2 \times 10^{-7}$  spins/2 rings. On the other hand, the magnitude of the steady-state PA ( $|\Delta T/T| \sim 5 \times 10^{-4}$ ) corresponds to an estimated density of defects of order  $10^{-3}$  defect/2 rings (see Sec. IV). Therefore the ratio of photoexcited defects with spins to the total number of defects photoexcited is less than  $2 \times 10^{-4}$ . Consideration of other effects may reduce this upper limit. For example, the long-time growth of the number of spins associated with the ME feature upon photoexcitation may mask a small contribution. However, we can safely put an upper limit of the branching ratio for the number of shorter-lived defects with spin created upon photoexcitation compared to total defects created as 0.1.

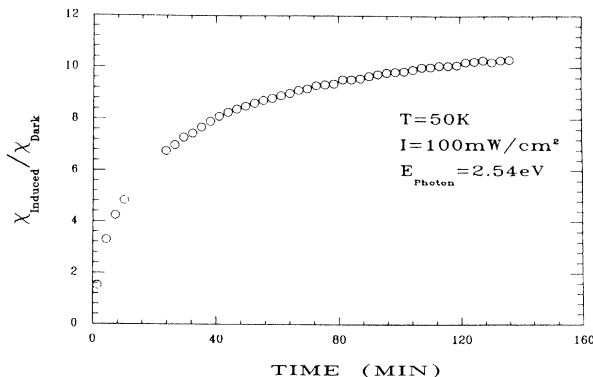


FIG. 17. Change in the double integral of the ESR spectrum divided by the dark ESR signal as a function of illumination time. The data were taken at a sample temperature of 50 K, laser intensity of  $100 \text{ mW/cm}^2$ , and photon energy of 2.54 eV.

## IV. DISCUSSION

### A. Ground state

We associate the observed  $\sim 2.3$ -eV absorption peak with the absorption across the predicted<sup>23</sup> Peierls gap. Calculations by Brédas *et al.*<sup>23</sup> indicate that 60% of the Peierls gap derives from the bond-order dimerization and 40% from the ring-torsion-angle dimerization. The two absorption peaks at 3.8 and 4.6 eV are attributed to the  $\pi-\pi^*$  gap absorptions centered primarily at benzenoid and quinoid rings, respectively. The mode at  $848\text{ cm}^{-1}$  is assigned<sup>33-35</sup> as the  $b_{3u}$  C-H out-of-plane vibrational mode; the  $1106\text{-cm}^{-1}$  mode is assigned as the  $b_{2u}$  ring-stretching mode. The  $1164\text{ cm}^{-1}$  mode is either due to the  $a_g$  C-H in-planar deformation or C-NH stretching vibration. The  $1318\text{-cm}^{-1}$  mode is attributed to the  $b_{1u}$  stretching radial vibrational mode. The  $1485\text{-cm}^{-1}$  mode is assigned as the  $b_{1u}$  C-C stretching vibration. The  $1585\text{-cm}^{-1}$  mode is assigned as either as  $a_g$  C-C ring-stretching or  $b_{1u}$  C-C ring-stretching vibrations.

It is interesting to note that in the spectrum of EB shown in Fig. 4 several weak IR modes of PNB are observed. For example, features such as the shoulder at  $\sim 848\text{ cm}^{-1}$  and weak peaks at  $1215\text{ cm}^{-1}$  in the spectrum of EB are present in the spectrum of PNB as strong peaks. The presence of these features in EB is consistent with the EB samples being somewhat overoxidized when samples are exposed to air.<sup>7</sup>

### B. Excited defect states

#### 1. Multiple order parameters

Several models have been proposed to study the excited states of pernigraniline base in light of electron-phonon coupling and electron ring-angle-torsion coupling. The two contributions give important insights on the nature of the defects of pernigraniline base, though a more detailed approach would include coupling between the two terms.

dos Santos and Brédas<sup>1</sup> studied the nonlinear excitations of PNB by a Su-Schrieffer-Heeger-like model based on effective bond-length-bond-order parameters. In other words, only an order parameter  $u$  is explicitly treated in the model, while order parameters  $\Psi_0$  and  $\delta$  are suppressed. In this model, the electronic resonance integrals between N-N atoms are parametrized by using a renormalization procedure to suppress the  $C_6$  rings. The site energies of C and N atoms are fitted to the valence-effective Hamiltonian (VEH) pseudopotential band-structure calculations by a parametrized tight-binding model.

Two types of charged solitons are found<sup>1</sup> to be stable in pernigraniline base: (a) The type-I soliton has rings around the defect center that have the benzenoid geometry, which introduces a localized state 0.11 eV below the Fermi level; (b) the type-II soliton has rings around the defect center that are of quinoid structure; its defect level is 0.06 eV above the Fermi level. The center of each type of defect corresponds to a nitrogen atom.

The most stable configuration for a soliton-antisoliton pair corresponds to the type-I soliton level being doubly occupied ( $S_{BB}^-$ ) and the type-II soliton level empty ( $S_{QQ}^+$ ), with a total creation energy of 0.64 eV. A fractional charge of  $-0.52|e|$  is found around the type-I soliton and an opposite charge of  $0.52|e|$  around the type-II soliton. The most stable configuration is thus nonmagnetic, contrary to the situation of a neutral soliton excitation in *trans*-(CH)<sub>x</sub>. Taking the effective bond-order changes<sup>1</sup> as the only contribution, the mass of the soliton can be estimated to be  $\sim 5m_e$ , which is on the same order as that of the bond-order soliton in *trans*-(CH)<sub>x</sub>. Su and Epstein have shown<sup>4</sup> that the neutral soliton  $S_{BB}^0$  is also stable as a result of the absence of charge-conjugation symmetry. Long *et al.*<sup>36</sup> have observed this soliton in solution EPR experiments, while Coplin *et al.*<sup>30</sup> have observed it in long-lived photoinduced-absorption studies. Polarons described by effective bond-order changes were described by dos Santos and Brédas<sup>1</sup> for PNB, while earlier work of Ginder and Epstein<sup>3</sup> applied the concept of a ring-rotation polaron to LEB. dos Santos and Brédas and Su and Epstein have found that upon addition or removal of an electron or hole to PNB, the most stable excitation is a polaron. They further concluded that bipolarons are not stable in PNB.

Ginder and Epstein<sup>2</sup> utilized a Hückel Hamiltonian to describe the ground states of LEB and PNB in terms of ring-torsion-angle order parameters. Although the ring-torsional angle  $\Psi_0 \sim 56^\circ$  for LEB estimated by this method is too large for PNB,<sup>23,28</sup> the ring-torsional defects introduced by this model are still useful for understanding the steric interaction between rings. These steric interactions are believed to repel adjacent rings to opposite ring angles away from the plane defined by the nitrogen atoms. A stable ring-torsional hole-polaron solution is found in their model for LEB. The hole-polaron solution  $P_B^+$  corresponds to a single energy level split off into the band gap by an energy  $\epsilon_P \approx 0.8$  eV from the valence band. The center  $C_6$  ring of the defect has its ring-torsion angle tilted toward the plane of N atoms. The magnitude of this ring twisting is found to be  $\sim 15^\circ$ , which is rather significant. The defect mass of such a hole polaron is estimated by Ginder and Epstein to be as large as 50 times the free-electron mass ( $m_e$ ), very different from that of a conventional polaron which has a defect mass of order  $m_e$ . McCall *et al.*<sup>21</sup> and Stafström, Sjögren, and Brédas<sup>37</sup> have suggested that a  $P_B^+$  may be bound to a quinoid group to form a  $P_{BQ}^+$  with a single polaron energy level of  $\sim 1.5$  eV in the gap.

For PNB, the ring-torsion angles for benzenoid and quinoid rings are quite different (estimated<sup>23</sup> as  $\Psi_1 \sim 60^\circ$  for the benzenoid rings and  $\Psi_2 \sim 0^\circ$  for the quinoid rings). To emphasize the ring-torsional dimerization,<sup>2</sup> the average ring-torsion angle  $\Psi_0$  may be defined as

$$\Psi_0 = \frac{(\Psi_1 + \Psi_2)}{2} . \quad (9)$$

The benzenoid rings and quinoid rings are suggested to deviate from such an average angle by  $\delta$ . As noted above, Brédas *et al.*<sup>23</sup> determined that the contribution of

the  $u$  and  $\delta$  order parameters to the band gap are nearly equal.

Su and Epstein have calculated the energy spectra of positive and negative polarons in PNB (Fig. 18). Unlike the  $P_B^+$  of LEB, these polarons have two levels in the gap. However, because of charge-conjugation asymmetry, the  $P^+$  levels lie close to the band edges while the  $P^-$  levels are more isolated, with a transition between the two  $P^-$  levels of 1.5 eV.

The other  $P^-$  and  $P^+$  transitions are absent. This may be due to the effects of quantum fluctuations and static disorder in the Peierls gap. MacKenzie and Wilkins recently have shown<sup>38</sup> that these effects scale as the ratio of the Peierls gap ( $\sim 2.3$  eV for PNB) to the undistorted bandwidth [3.0 eV for LEB (Ref. 39)]. This suggests that the effect of the quantum fluctuations and static disorder are much greater in PNB than in *trans*-(CH)<sub>x</sub>.<sup>30</sup> The larger band tailing observed for PNB as compared to that of *trans*-(CH)<sub>x</sub> suggests that these disorder effects may indeed make the other polaron transitions unobservable or part of the broad photoinduced absorption on the low-energy side of the long-lived 1.5-eV peak.

Based on their energies, we assign the LE1 and LE2 transitions to those of the charged solitons and the 1.5-eV transition to that of negatively charged polarons  $P^-$ .

## 2. Lifetime of the defects

The two kinds of defects have different lifetimes. The LE features have lifetimes of  $\sim 100$  msec scale determined by the chopper frequency dependence measurements. In contrast, the lifetime of the ME feature is much longer, exceeding 24 h at 80 K.

For long-lived PA experiments with continuous pump-light exposure of intensity of 250 mW/cm<sup>2</sup> for over several hours at 80 K, the magnitude of the PA signal ( $|\Delta T/T|$ ) for the ME feature asymptotes to  $\sim 0.4$ . A rough estimate of the defect density can be obtained as follows: The photoinduced absorption is related to the

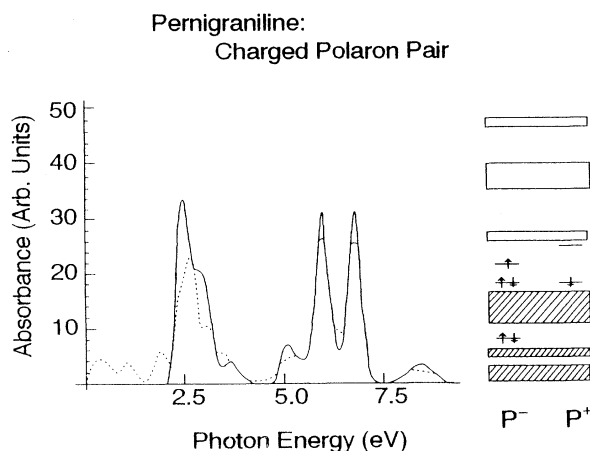


FIG. 18. Calculated absorption spectrum of a PNB chain in the ground state (solid line) and with a polaron pair (dotted line). The energy-level diagram of the polarons is shown to the right of the absorption curves (from Ref. 4).

change of optical-absorption coefficient by  $|\Delta T/T| = \Delta\alpha_{PA}/\alpha_{pump}$ , where  $\Delta\alpha_{PA}$  is the photoinduced change of the optical-absorption coefficient and  $\alpha_{pump}$  is the optical-absorption coefficient at the pump photon energy. The parameter  $\alpha_{pump}$  was estimated to be  $\sim 10\,000$  cm<sup>-1</sup> by measuring the absorbance of a PNB thin film and its film thickness. Thus  $\Delta\alpha_{PA}$  is estimated to be  $\sim 4000$  cm<sup>-1</sup> for the long-lived defect. We then assume that the long-lived PA is due to polarons similar to that in emeraldine salt, which has one polaron per two rings. The change of the optical-absorption coefficient due to protonic acid doping of the emeraldine-base polymer,  $\Delta\alpha_{doping}$ , is estimated to be  $\sim 10\,000$  cm<sup>-1</sup>. By comparing the quantity  $\Delta\alpha_{doping}$  due to doping to  $\Delta\alpha_{PA}$  due to photoexcitation, the concentration of the long-lived defects at saturation is estimated to be one defect per five to six rings.

For the short-lived defect, the PA signal is of the order of  $|\Delta T/T| \sim 5 \times 10^{-4}$ , which can be readily converted into a density of  $10^{-3}$  defect/2 rings by comparing with the long-time PA signal.

## 3. Photoinduced IRAV modes

Long-lived photoinduced IRAV modes for PNB have two major features at 1153 and 1554 cm<sup>-1</sup>. These features are assigned as the formerly Raman-active modes of C-H in-plane deformation (1181 cm<sup>-1</sup>) and  $a_g$  C-C stretching of the benzenoid ring and C-C stretching of the quinoid ring (1622 cm<sup>-1</sup>) becoming IR active due to a symmetry break along the one-dimensional chain. However, the long-lived IRAV mode at 1477 cm<sup>-1</sup> is unique to PNB and is absent in LEB and EB.<sup>21,29</sup> The fact that this vibrational mode is close in frequency to the Raman-active mode at 1479 cm<sup>-1</sup> (C=N stretching and C-C stretching) allows us to attribute this Raman-active mode as the origin at 1477 cm<sup>-1</sup> due to the symmetry breaking. If this assignment is correct, this Raman-active mode directly modulates the Peierls gap, which is proportional to the bond-length dimerization.

Short-lived photoinduced IRAV modes of PNB are very different from that of the long-lived ones as shown in Fig. 8. Four new strong PA modes are observed at 1100, 1220, 1320, and 1580 cm<sup>-1</sup>. None of these features were observed in the long-lived PA. We suggest that these PA modes originate from Raman-active modes at 1163 cm<sup>-1</sup> (C-H in-plane deformation), 1223 cm<sup>-1</sup> (C-N stretching and C-C stretching), 1321 cm<sup>-1</sup> (C-H radial stretching), and 1617 cm<sup>-1</sup> (C-C ring stretching). The choice of Raman-active modes of C-C stretching at 1617 cm<sup>-1</sup> in the fitting reflects that the short-lived IRAV modes (1580 cm<sup>-1</sup>) are higher in vibrational frequency than that of the long-lived one (1554 cm<sup>-1</sup>).

Proper caution must be made to the above assignment: Only limited information of Raman spectroscopy of polyaniline is available. No definitive assignments can be made unless experimental evidence confirms the correspondence of these Raman and IRAV modes. Further comparative studies of IR-absorption, Raman, and photoinduced-absorption spectroscopy are needed on

better quality samples (higher crystallinity, better control of oxidation states, etc.).

#### 4. Amplitude-mode formalism analysis

Following the amplitude-mode formalism (AMF) proposed by Horovitz *et al.*<sup>27</sup> in studying *trans*-(CH)<sub>x</sub>, we studied the long- and short-lived defects with their associated IRAV modes. For the long-time PA experiment of PNB, the primary PA features observed at 1153, 1477, and 1554 cm<sup>-1</sup> are regarded as formerly Raman-active modes<sup>34</sup> at 1163, 1479, and 1559 cm<sup>-1</sup> that become IR active due to symmetry breaking. A three-oscillator phonon Green's function was constructed for the long-lived photoinduced IRAV modes. Using the Green's function

$$D_0(\omega) = -\frac{1}{1-\alpha}, \quad (10)$$

one can determine the pinning potential  $\alpha$  as well as the bare phonon modes of the polymer. The same Green's function  $D_0(\omega)$  can also be used to determine the resonant Raman-scattering modes of the polymer, with the effective coupling constant  $\tilde{\lambda}$  as the adjustable parameter i.e.,

$$D_0(\omega) = -\frac{1}{1-2\tilde{\lambda}}. \quad (11)$$

We construct three bare phonon modes  $\omega_0^{(1)}$ ,  $\omega_0^{(2)}$ , and  $\omega_0^{(3)}$  and two free parameters  $\lambda_1/\lambda$  and  $\lambda_2/\lambda$  (with  $\lambda_3$  constrained by  $\lambda_3/\lambda = 1 - \lambda_1/\lambda - \lambda_2/\lambda$ ). Using this fitting procedure (Fig. 19), we obtain values of  $\alpha \sim 0.74$  and  $2\tilde{\lambda} \sim 0.76$  for the long-lived defect.

The IRAV modes of the short-lived photoinduced defect of PNB present at 1100, 1220, 1320, and 1580 cm<sup>-1</sup> arise from symmetry breaking of the *para*-disubstituted benzene rings due to formation of predominantly bond-order solitons. Hence the formerly Raman-active modes at 1163, 1223, 1321, and 1617 cm<sup>-1</sup> become IR active. A four-oscillator phonon Green's function was used to fit the data yielding an effective electron-phonon coupling parameter  $2\tilde{\lambda} \sim 0.66$  for the short-lived defect in PNB and a pinning parameter  $\alpha \sim 0.58$  (Fig. 20). It is noted

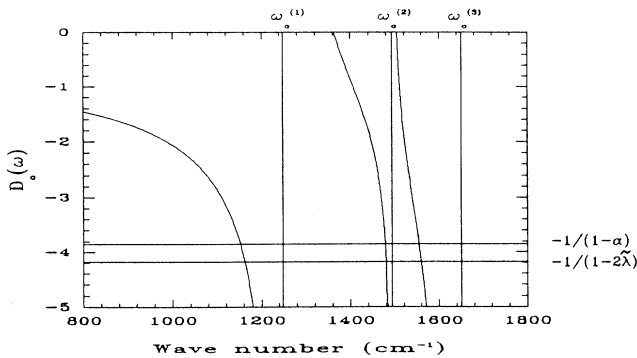


FIG. 19. Fitting of the long-lived photoinduced IRAV modes using the amplitude-mode formalism. The curves are plots of  $D_0(\omega)$ , the vertical lines represent the bare phonon modes (three modes in this case), and the horizontal lines represent the values of  $-1/(1-\alpha)$  and  $-1/(1-\tilde{\lambda})$ .

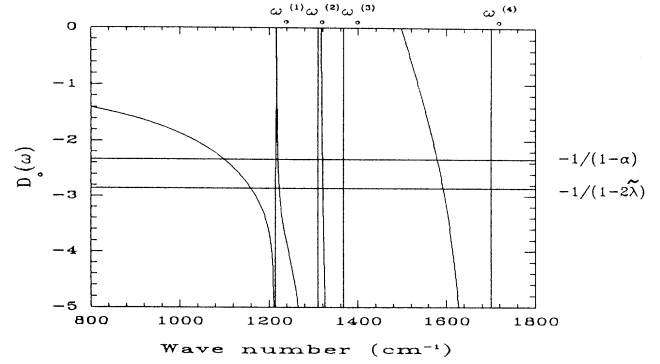


FIG. 20. Fitting of the short-lived photoinduced IRAV modes using the amplitude-mode formalism. The curves are plots of  $D_0(\omega)$ , the vertical lines represent the bare phonon modes (four modes in this case), and the horizontal lines represent the values of  $-1/(1-\alpha)$  and  $-1/(1-\tilde{\lambda})$ .

that the pinning parameter for PNB is larger than that of polyacetylene ( $\sim 0.06$ ) and polythiophene ( $\sim 0.31$ ). Also, it is seen that the short-lived defect is less pinned than the long-lived defect.

The AMF can also be used to estimate the defect masses. The integrated oscillator strength of the IRAV modes can be expressed as

$$I_v = \frac{\pi \rho e^2}{2 M_d} \frac{\Omega_1^2}{\Omega_0^2}, \quad (12)$$

where  $\rho$  is the charge density of the defect,  $M_d$  is the mass of the defect, and  $\Omega_1^2$  and  $\Omega_0^2$  are two quantities related to the bare phonon frequencies:

$$\Omega_1^2 = \sum_n \frac{\lambda_n}{\lambda} (\omega_n^0)^2, \quad (13)$$

$$\Omega_0^{-2} = \sum_n \frac{\lambda_n}{\lambda} (\omega_0^0)^{-2}. \quad (14)$$

On the other hand, the oscillator strength of the electronic transition  $I_s$  is given by

$$I_s = \frac{2.8 \rho e^2}{m^*}, \quad (15)$$

where  $m^*$  is the electron-band effective mass. Therefore the defect mass ( $M_d$ ) can be expressed as

$$\frac{M_d}{m^*} = \frac{\pi I_s \Omega_1^2}{5.6 I_v \Omega_0^2}. \quad (16)$$

The ratio of the electronic and IRAV oscillator strengths for the ME feature in the long-time PA experiment is calculated to be  $\sim 3000$ , while this ratio is estimated to be  $\sim 80$  for the LE features in the near-steady-state PA experiment. Using a band effective mass of  $0.14 m_e$  for PNB, the defect masses are estimated to be  $\sim 300 m_e$  for the long-lived defects and  $(5-10) m_e$  for the short-lived defects. This confirms that the polaron state associated with the 1.5-eV absorption has a substantial ring-torsion-angle order-parameter deformation associated with it. However, the relatively light mass of the low-

energy charged (solitonlike) feature suggests that it is primarily determined by the bond-length order parameter despite the expected ring-torsion coupling.

Before closing this section, a caution about the calculation of defect mass for the ring-torsional polaronlike defect must be given. The large defect mass ( $\sim 300m_e$ ) of the polaronlike defect is obtained by comparing the electronic excitations at 1.5 eV and vibrational excitations. However, as these infrared-active modes are assigned as C-C, C-N, and C-H stretching and deformation vibrations, the defect mass calculated in such a way reflects the coupling of ring-torsional motions of the defect to the bond-length order parameter. Attempts at direct observation of photoinduced torsional modes have, as yet, been unsuccessful.

### 5. Spin of the defects

The LESR experiments demonstrated that the long-lived defect has a spin of  $\frac{1}{2}$ , while the short-lived defect is spinless. The results agree with the assignment of the short-lived defects to charged solitons and the long-lived defect to charged polarons and neutral solitons.

## V. CONCLUSIONS

We conclude that pernigraniline base, which is in the highest oxidation state of polyaniline, is a one-dimensional  $\pi$ -conjugated polymer with a degenerate Peierls ground state. It has three order parameters operative, namely, the bond-length dimerization  $u$ , the average phenyl ring angle  $\Psi_0$ , and the phenyl ring-angle dimerization  $\delta$ . The broadening of the band-edge absorption may reflect the increased sensitivity of this system to disorder.

Direct absorption and photoinduced absorption including near-steady-state and long-time techniques, as well as the LESR technique, were employed to study the photoexcited defect states of pernigraniline base. Two kinds

of photoinduced defects were observed below 1.5 eV at low temperatures. The first kind of defect, which exhibits two photoinduced-absorption peaks at  $\sim 1.1$  and  $\sim 1.3$  eV, is relatively short lived with a lifetime of  $\sim 100$  msec. The second kind of defect, which exhibits one photoinduced absorption at  $\sim 1.5$  eV with a low-energy tail, is relatively long lived with a lifetime of  $\sim 24$  h. The short-lived defect has a set of photoinduced infrared-active vibrational modes at 1100, 1220, 1320, and 1559  $\text{cm}^{-1}$ , while the long-lived defect has a different set of photoinduced infrared-active vibrational modes at 1153, 1477, and 1554  $\text{cm}^{-1}$ . Light-induced electron-spin-resonance measurements demonstrate that the short-lived defects are spinless, whereas the long-lived defects have a spin of  $\frac{1}{2}$ .

Within the amplitude-mode formalism, the mass of the short-lived defect is estimated to be  $(5-10)m_e$ , while the mass of the long-lived defect is estimated to be much larger. Pinning parameters  $\alpha \sim 0.58$  and  $0.74$  are estimated for the short- and long-lived defects, respectively, with effective electron-phonon coupling constants  $2\tilde{\lambda} \sim 0.66$  and  $0.76$ .

We conclude that the short-lived defects originate from excitation of charged soliton-antisoliton pairs that involve primarily the order parameter  $u$ , while the long-lived defects associated with the 1.5-eV photoinduced absorption originate from negative polaronlike excitations of the Peierls gap with significant  $\Psi_0$  and  $\delta$  contributions to the order parameters. Further study will provide insight into the effects of interaction among order parameters in a complex degenerate Peierls system.

## ACKNOWLEDGMENTS

We wish to thank K. A. Coplin, J. M. Ginder, M. E. Józefowicz, and H. J. Ye for their contributions to this work. This work was supported in part of the Defense Advanced Research Projects Agency through a contract monitored by the U.S. Office of Naval Research and the Office of Naval Research.

\*Present address: Department of Physics, University of Utah, 201 JFB, Salt Lake City, UT 84112.

†Present address: Department of Physics, Louisiana Tech. University, Ruston, LA 71272.

‡Present address: Room A 181, Building 200, Argonne National Laboratory, Argonne, IL 60439.

§Present address: Rohm and Haas Company, 727 Morristown Road, Spring House, PA 19477.

||Present address: Proctor and Gamble Corporation, Cincinnati, OH.

<sup>1</sup>M. C. dos Santos and J. L. Brédas, *Phys. Rev. Lett.* **62**, 2499 (1989); **64**, 1185 (1990); *Synth. Met.* **29**, E321 (1989).

<sup>2</sup>J. M. Ginder and A. J. Epstein, *Phys. Rev. Lett.* **64**, 1184 (1990).

<sup>3</sup>J. M. Ginder and A. J. Epstein, *Phys. Rev. B* **41**, 10 674 (1990).

<sup>4</sup>W. P. Su and A. J. Epstein, *Phys. Rev. Lett.* **70**, 1497 (1993); W. P. Su, J. Kim, and A. J. Epstein, *Synth. Met.* **57**, 4326 (1993).

<sup>5</sup>A. G. Green and A. E. Woodhead, *J. Chem. Soc. Trans.* **97**, 2388 (1910); **101**, 1117 (1912).

<sup>6</sup>See, for example, *Proceedings of the International Conference on the Science and Technology of Synthetic Metals*, Gothenberg, Sweden, August 1992 [*Synth. Met.* **57-57**, (1993)]; Tübingen, Germany, Sept. 1990 [*Synth. Met.* **41-43**, (1991)]; Santa Fe, NM, June 1988 [*Synth. Met.* **27-29**, (1989)].

<sup>7</sup>A. G. MacDiarmid and A. J. Epstein, *Faraday Discuss. Chem. Soc.* **88**, 317 (1989).

<sup>8</sup>J. C. Chiang and A. G. MacDiarmid, *Synth. Met.* **13**, 193 (1986).

<sup>9</sup>J. M. Ginder, A. F. Richter, A. G. MacDiarmid, and A. J. Epstein, *Solid State Commun.* **63**, 97 (1987).

<sup>10</sup>S. Stafström, U. L. Brédas, A. J. Epstein, H. S. Woo, D. B. Tanner, W. S. Huang, and A. G. MacDiarmid, *Phys. Rev. Lett.* **59**, 1464 (1987).

<sup>11</sup>A. G. MacDiarmid, S. K. Manohar, J. G. Masters, Y. Sun, H. Weiss, and A. J. Epstein, *Synth. Met.* **41**, 621 (1991).

- <sup>12</sup>Z. H. Wang, C. Li, E. M. Scherr, A. G. MacDiarmid, and A. J. Epstein, *Phys. Rev. Lett.* **66**, 1745 (1991); Z. H. Wang, E. M. Scherr, A. G. MacDiarmid, and A. J. Epstein, *Phys. Rev. B* **45**, 4190 (1992).
- <sup>13</sup>H. L. Wu and P. Phillips, *Phys. Rev. Lett.* **66**, 1366 (1991).
- <sup>14</sup>K. Mizoguchi, M. Nechtschein, J.-P. Travers, and C. Menardo, *Phys. Rev. Lett.* **63**, 66 (1989).
- <sup>15</sup>J. P. Puget, M. E. Józefowicz, A. J. Epstein, X. Tang, and A. G. MacDiarmid, *Macromolecules* **24**, 779 (1991).
- <sup>16</sup>B. Lundberg, W. R. Salaneck, and L. Lundstrom, *Synth. Met.* **21**, 143 (1987); F. Wudl, R. O. Angus, F. L. Lu, P. M. Allemand, D. J. Vachon, M. Nowak, Z. X. Liu, and A. J. Heeger, *J. Am. Chem. Soc.* **109**, 3475 (1987).
- <sup>17</sup>M. G. Roe, J. M. Ginder, P. E. Wigen, A. J. Epstein, M. Angelopoulos, and A. G. MacDiarmid, *Phys. Rev. Lett.* **60**, 2789 (1988).
- <sup>18</sup>Y. Sun, A. G. MacDiarmid, and A. J. Epstein, *J. Chem. Soc. Chem. Commun.* **1990**, 529 (1990).
- <sup>19</sup>J. G. Masters, Y. Sun, A. G. MacDiarmid, and A. J. Epstein, *Synth. Met.* **41**, 715 (1991).
- <sup>20</sup>T. Holstein, *Ann. Phys. (N.Y.)* **8**, 325 (1959); **8**, 343 (1959).
- <sup>21</sup>R. P. McCall, J. M. Ginder, J. M. Leng, H. J. Ye, S. H. Manohar, J. M. Masters, G. E. Asturias, A. G. MacDiarmid, and A. J. Epstein, *Phys. Rev. B* **41**, 5202 (1990).
- <sup>22</sup>Y. Cao [*Synth. Met.* **35**, 319 (1990)] reported chemical doping of PNB synthesized by a different route. Though the UV-visible-near-infrared spectra show some evidence of in-gap absorption due to chemical doping, substantial controversy remains concerning the irreversible reaction of the chemical dopant (iodine substitution) with PNB [A. G. MacDiarmid *et al.* (Ref. 11); Y. Sun, A. G. MacDiarmid, and A. J. Epstein, *Bull. Am. Phys. Soc.* **36**, 781 (1991)].
- <sup>23</sup>J. L. Brédas, C. Quattrocchi, J. Libert, A. G. MacDiarmid, J. M. Ginder, and A. J. Epstein, *Phys. Rev. B* **44**, 6002 (1991).
- <sup>24</sup>J. M. Leng, R. P. McCall, K. R. Cromack, J. M. Ginder, H. J. Ye, Y. Sun, S. K. Manohar, A. G. MacDiarmid, and A. J. Epstein, *Phys. Rev. Lett.* **68**, 1184 (1992).
- <sup>25</sup>J. M. Leng, J. M. Ginder, R. P. McCall, H. J. Ye, A. J. Epstein, Y. Sun, S. K. Manohar, and A. G. MacDiarmid, *Synth. Met.* **41**, 1311 (1991).
- <sup>26</sup>K. R. Cromack, A. J. Epstein, J. G. Masters, Y. Sun, and A. G. MacDiarmid, *Synth. Met.* **41**, 641 (1991).
- <sup>27</sup>B. Horovitz, *Solid State Commun.* **41**, 729 (1982); B. Horovitz, Z. Vardeny, E. Ehrenfreund, and O. Brafman, *Synth. Met.* **9**, 215 (1984).
- <sup>28</sup>M. E. Józefowicz, A. J. Epstein, J. P. Pouget, J. G. Masters, A. Ray, Y. Sun, X. Tang, and A. G. MacDiarmid, *Synth. Met.* **41**, 723 (1991).
- <sup>29</sup>R. P. McCall, J. M. Ginder, J. M. Leng, K. A. Coplin, H. J. Ye, A. J. Epstein, G. E. Asturias, S. K. Manohar, J. G. Masters, E. M. Scherr, Y. Sun, and A. G. MacDiarmid, *Synth. Met.* **41**, 1329 (1991).
- <sup>30</sup>K. A. Coplin, J. M. Leng, R. P. McCall, A. J. Epstein, S. K. Manohar, Y. Sun, and A. G. MacDiarmid, *Synth. Met.* **55**, 7 (1993); K. A. Coplin, S. Jasty, S. M. Long, S. K. Manohar, Y. Sun, A. G. MacDiarmid, and A. J. Epstein (unpublished).
- <sup>31</sup>M. E. Jozefowicz, A. J. Epstein, and A. G. MacDiarmid, *Synth. Met.* **59**, 123 (1993); M. E. Jozefowicz, Ph.D. thesis, The Ohio State University, 1991.
- <sup>32</sup>K. R. Cromack *et al.* (unpublished); K. R. Cromack, Ph.D. thesis, The Ohio State University, 1991.
- <sup>33</sup>R. P. McCall *et al.* (unpublished).
- <sup>34</sup>Y. Furukawa, T. Hara, Y. Hyodo, and I. Harada, *Synth. Met.* **16**, 189 (1986); I. Harada, Y. Furukawa, and F. Ueda, *ibid.* **29**, E303 (1989).
- <sup>35</sup>G. Varsányi, *Vibrational Spectra of Benzene Derivatives* (Academic, New York, 1969).
- <sup>36</sup>S. M. Long, K. R. Cromack, Y. Sun, A. G. MacDiarmid, and A. J. Epstein (unpublished).
- <sup>37</sup>S. Stafström, B. Sjögren, and J. L. Brédas, *Synth. Met.* **29**, E219 (1989).
- <sup>38</sup>R. MacKenzie and J. W. Wilkins, *Phys. Rev. Lett.* **69**, 1085 (1992).
- <sup>39</sup>D. S. Boudreaux, R. R. Chance, J. F. Wolf, L. W. Shacklette, J. L. Brédas, B. Thémans, J. M. André, and R. Silbey, *J. Chem. Phys.* **85**, 4584 (1986).